High-precison, fully integrated optical angle measuring sensor in standard CMOS technology

Tobias Schwanke, Johannes Fromme and Jürgen Oehm
Analogue Integrated Circuits Research Group, Ruhr-University Bochum, Germany

***Abstract*—This paper presents a system for high-precision optical measurement of the angle of incidence of light that offers significant improvements over previous methods. By leveraging recent improvements in analog circuit technology alongside a novel digital post-processing technique, the system demonstrates a significant enhancement in overall. A comprehensive analysis of both the optical components and the digital output is provided. The proposed system delivers a highly precise, nearly drift-free, and robust against statistical parametric tolerance influences digital angular signal and offers the user the flexibility to choose between conversion rate and resolution, allowing easy customization of the integration solution to the specific requirements of an application. The measurement system presented here is designed for high-precision refractometric measurements with regard to the optical system setup. Resolutions of up to more than ± 14.5 Bits can be achieved.**

***Index Terms*—angle measurement, fully integrated optical sensor technology, high-precision sensory CMOS optics, refractometer, drift-free optical CMOS sensors, field-of-view.**

I. Introduction

Optical CMOS sensors have become a versatile tool, widely used across various fields for their ability to measure not only light intensity with high spatial resolution, but also other critical optical properties. One such property is the optical angle of incidence, which holds significant importance for numerous technical applications. In space exploration, for example, accurate sun position information is essential for satellite orientation and control. This is especially critical for nanosatellites, where ultra-compact lightweight optical angle sensors are pivotal in maintaining the efficiency and performance of space missions [1], [2]. Another significant application of the presented sensor is (transmitted) light refractometry [3], a technique commonly used in various scientific and industrial fields to measure the refractive index of materials. The refractive index is a fundamental material property that describes how light propagates through a given medium. In transmitted light refractometry, the refractive index of a sample is determined by analyzing the angular change that occurs when light passes from one medium (typically air or another transparent material) into the material under examination. The sensor introduced in this paper has been specifically optimized for this purpose by accurately detecting the angle of incidence and the corresponding changes in refraction. Previous investigations have demonstrated the functional principle of the optical sensor, its robustness even when using light sources with a strong gradient in the illumination cone at a minimum distance to the sensor and its design variability with regard to the detection angle range [4]–[6]. These studies have laid the foundation for understanding the sensor's performance under varying optical conditions. In contrast, this article concentrates on the further development of the analogue/digital evaluation circuit in order to increase the achievable precision to a maximum in conjunction with a new type of signal processing. The fundamental concept behind these developments is the generation of a signal that is devoid of both drift and 1/f noise. This signal can then be averaged over an extended duration, thereby ensuring maximal precision.

II. Working Principle

A. System architecture

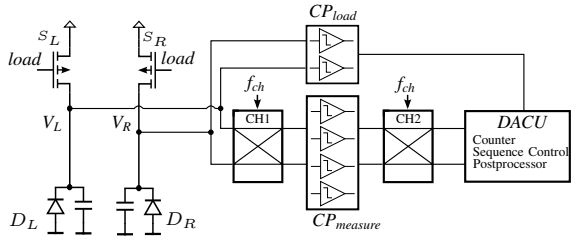

Fig. 1: New analogue/digital System architecture.

The system architecture, depicted in Fig. 1, consists of several key components: an optical angle sensor comprising the right and left photodiodes (D_R and D_L), a switching head (S_R and S_L), a chopping mechanism ($CH1$ and $CH2$), two comparator blocks (CP_{load} and $CP_{measure}$), and a digital arithmetic and control unit (DACU). The optical angle sensor employs a dual-photodiode configuration, where each photodiode converts the angle of incidence into angle-dependent photocurrents, aided by precision shading structures shown in Fig. 2. Additionally, the diodes are fabricated in the multi-quad

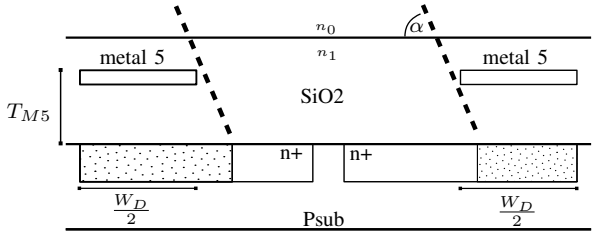

Fig. 2: Integrated monolithic optical angle of incidence sensor structure in a CMOS stack without illumination gradient compensation.

arrangement outlined in [5], which minimizes the impact of lighting gradients or silicon inhomogeneities. This specialized structure enables the use of light sources positioned very close to the chip, even when gradients are dispersed, such as in the

case of LEDs. Alternatively, light sources with nearly point-source characteristics may also be employed [4]. The resulting photocurrents, I_R and I_L, corresponding to the right and left photodiodes, respectively, are governed by the following relationship [6]:

$$I_L \propto \frac{W_D}{2} - T_{M5} \cdot \left(tan \left(arcsin \left(\frac{n_0}{n_1} sin\left(\alpha\right) \right) \right) \right) \quad (1)$$

$$I_R \propto \frac{W_D}{2} + T_{M5} \cdot \left(tan \left(arcsin \left(\frac{n_0}{n_1} sin\left(\alpha\right) \right) \right) \right) \quad (2)$$

In order to obtain an origin-symmetric angular characteristic, the following relationship must be applied to the two photocurrents. A negative angle α corresponds to a negative ratio of the photocurrents, thereby maintaining symmetry about the origin [5]:

$$r_i = \frac{I_L - I_R}{I_L + I_R} \ , \quad r_i = f(\alpha) \quad (3)$$

The relative related difference r_i of the photocurrents is a normalized measure for the angle of incidence of light α, for which the absolute value of the photocurrents no longer plays a role. The photocurrents generated by the photodiodes are used to discharge the pre-charged parasitic non-linear capacitances of the diodes D_L and D_R, whereby the initial pre-charging is carried out by the switching head (S_L and S_R). The non-linearity of the capacitances of the identical photodiodes plays no role for the r_i value if the discharge of the non-linear capacitances for both measurement paths is always only observed via the same fixed discharge points.

B. Comparator

The two comparator blocks shown schematically in Fig. 1 consist of a total of three different comparators per photodiode measurement path (see Fig. 3). The comparator CP_{load} monitors the pre-charging process and terminates the pre-charging process in its photodiode measurement path as soon as its reference voltage V_{load} is exceeded. Once the charging processes for both photodiode measurement paths are complete, the parasitic capacitances of both photodiodes are discharged. On the one hand, this ensures uniform and reliable charging of both photodiodes while simultaneously minimising the duration of the entire measurement cycle, which is made up of the duration of the charging time plus the maximum discharge time of the slower measurement path. Secondly, this configuration ensures that both measurement phases always start with the same constant potential regardless of the respective level of the photocurrents in the measurement paths. This means that comparatively higher measurement rates can now be achieved for the entire measurement sequence with much more robustly defined charging and discharging conditions than with the previous solutions. The remaining two comparators $CP_{measure}$ shown in Fig. 3, are used to detect the crossing of an upper and a lower switching threshold, $V_{ref,High}$ and $V_{ref,Low}$, respectively. The time taken for this process is recorded and serves as a measure of the photocurrent in a measurement path. Given that comparators inherently introduce a delay between threshold crossing and decision output, the use of two identical comparators to monitor the upper and lower thresholds effectively minimizes the impact of this delay on the timing between threshold crossings. The

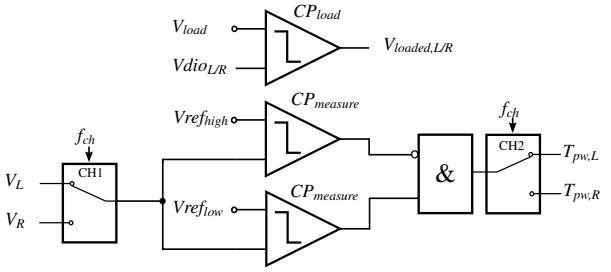

Fig. 3: Comparator arrangement of one measuring channel including the chopping mechanism.

output signals of the comparators for detecting the upper and lower switching thresholds are logically combined to generate a pulse signal with a pulse width T_{pw}. The pulse width of the signal corresponds to the discharge duration, and is therefore proportional to the photocurrent in a measurement path.

C. Chopping

The input transistors in the differential stage of a comparator in particular contribute significantly to 1/f noise currents, which then massively modulate the trigger threshold of a comparator. This 1/f noise is then reflected accordingly in the pulse width T_{pw}, which ultimately leads to a significant increase in noise in the sequence in the digital numerical output for the current angle value. To mitigate this problem, a chopping mechanism was implemented (see CH1 and CH2 in Fig. 1 and Fig. 3), which massively reduces the effects of 1/f noise in the comparators. With this approach, the effective positions of the comparators in the two measurement paths are swapped after each measurement. The summed count values of two consecutive measurements are then used to calculate the corresponding relative difference r_i from the counter values (see Eq. 4), which completely eliminates the effects of 1/f noise if the chopping rate is sufficient. The total acquisition time for an r_i value is therefore made up of two individual cycles, each with swapped comparator placement positions.

D. Digital arithmetic and control unit

Fig. 4 shows the core functionality of the 'Digital and Arithmetic Control Unit' (DACU). The DACU consists of the counters for the left and right measurement channels with the corresponding counter readings (CR_R and CR_L), an adder for optionally forming a sum of counter reading values from a total of M measurement repetitions, a divider calculation unit for calculating the relative related difference r_i from the counter reading values according to

$$r_i = \frac{CR_R - CR_L}{CR_L + CR_R} \quad (4)$$

and a mean value calculation unit for calculating the running mean value $\overline{r_i}$ from sequences of the running r_i calculations with the sample size N. The comparatively complex calculation of r_i values always takes place within a single measurement

cycle. According to the circuit described above, the r_i values are calculated identically according to Eq. 3 and Eq. 4, because the following applies: $CR_R \propto 1/I_R$ and $CR_L \propto 1/I_L$.

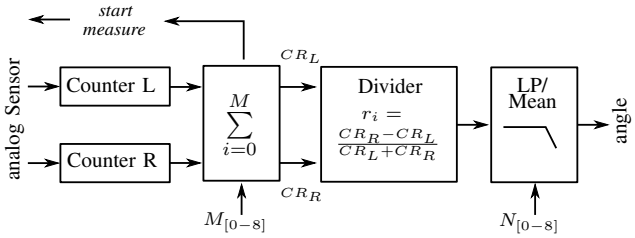

Fig. 4: DACU

The pulse width T_{pw} of the output signal generated by the analog section through the action of the comparators is counted with 170 MHz counters. The ratio between the pulse width and the fixed operating frequency of the counters can lead to such low counts with very strong illumination of the photodiodes that the number of significant digits is not sufficient for the required task of a sufficiently accurate r_i calculation (with e.g. at least 16-bit numerical accuracy). To counter this limitation, an adjustable number M of measurement repetitions can be carried out so that the accumulation of the counts of the M individual measurements finally leads to the respective sum values that are necessary to be able to carry out a sufficiently accurate r_i calculation. The counting results obtained from this summation process are then entered into a divider calculation unit, which calculates the corresponding angle information r_i. To further reduce the remaining noise (essentially the effects of the thermal noise contributions of the photodiodes and the transistors of the input stage of the respective comparators) in the sequence of r_i values, the mean value can then always be formed from a sequence of N r_i measurements. The noise in $\overline{r_i}$ then decreases further with $\sqrt{N}$. The comparatively short period of time required to calculate the individual r_i values from the count rate values CR_R and CR_L prevents slow gradients of any kind (e.g. in the ambient temperature and/or in the operating temperature of the light sources themselves) from influencing the calculation values of r_i and also increases the effectiveness of the chopping mechanism. A further increase in measurement precision with regard to noise can therefore be achieved by calculating the mean values $\overline{r_i}$ continuously over time from the time sequence of the calculated r_i values with a sample size of N. The theoretical maximum achievable $\overline{r_i}$ accuracy is ultimately given by the numerical accuracy of the r_i calculations. Another limitation is of course the measurement duration T_{conv} for $\overline{r_i}$, as a maximum value for T_{conv} is specified in every technical application. The following applies to the total measurement duration T_{conv} for $\overline{r_i}$, calculated from M measurement repetitions and N individual calculations r_i:

$$T_{conv} = (T_{pw} + T_{setup}) \cdot N \cdot M \tag{5}$$

The setup time T_{setup} consists of the charging time of the parasitic capacitance and the time needed to reach the measurement window in the voltage range (V_{load} to $V_{ref_{high}}$).

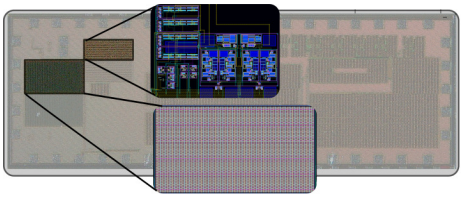

Fig. 5: Chip Foto with the analouge part and the two Photodiodes.

III. Measurement Results

The circuit was fabricated in the UMC 180 nm standard CMOS technology. The chip was illuminated with a 590 nm photodiode beam focused through a lens. The digital part of the circuit was developed on a VHDL basis and synthesized and tested on a FPGA for code optimization. It is part of the planned overall CMOS integration solution with even higher counting frequencies for the counters. A photo of the fabricated chip, highlighting the analog circuitry and the photosensitive areas, is shown in Fig. 5.

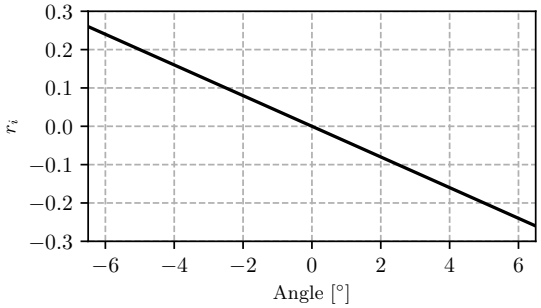

Fig. 6: Linear region of the angular characteristic curve.

In Fig. 6, the linear region of the sensor's characteristic curve is shown. The angle detection range intended for the application of refractometric measurements was deliberately limited in order to be able to precisely resolve the finest angle changes. Accordingly, a very linear angle detection range of $\pm 6.5°$ can be reliably detected with a digital resolution of up to ± 14.5 Bits. However, it should be noted that this high digital precision can also be achieved in conjunction with larger linear angle detection ranges (e.g. $\pm 45°$, see [6]). In this case, the absolute angular resolution is correspondingly lower.

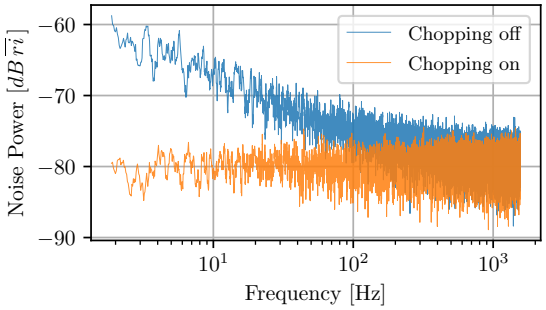

Fig. 7: FFT of the measurement signal r_i with and without chopping.

In order to test the effect of the chopping mechanism shown in Fig. 3, two comparative measurements were carried out: one with and one without the chopping mechanism activated. An FFT was carried out for both cases, the results of which are shown in Fig. 7. It can be clearly seen that when the chopping mechanism is activated, the 1/f noise of the comparators is largely suppressed and only white noise remains.

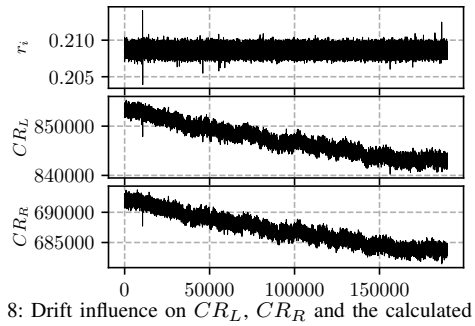

Fig. 8: Drift influence on CR_L, CR_R and the calculated r_i values.

To demonstrate the drift-suppressing effect of the r_i normalization in the DACU, a series of measurements was carried out over a period of 2 hours (Fig. 8). During this period, the temperature-related drift in the values of the respective counter readings CR_L and CR_R can be clearly seen. It is mainly due to operating temperature fluctuations of the system components. The relative related difference r_i calculated 'in time' in the DACU from the individual meter measurements no longer show this drift, which proves the effectiveness of the method.

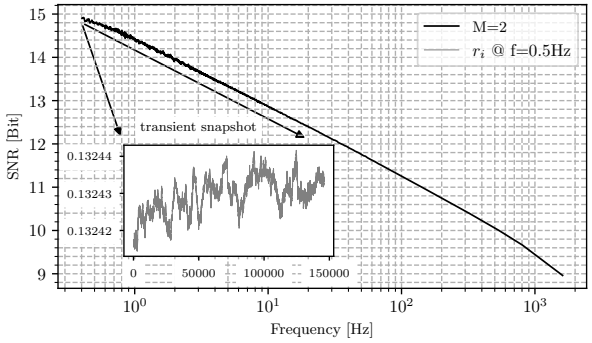

Fig. 9: Resolution vs. measurement rate at $r_i = 0.261/6.493°$.

The sensor concept allows trading off high measurement rates with reduced precision against low rates with increased precision by selecting appropriate M and N. Fig. 9 shows the relation between measurement frequency and resolution. Measurements were taken at the most extreme angular position of the linear region, where the photocurrent within one channel is minimal—resulting in the lowest frequency and poorest signal-to-noise ratio. Over 100,000 samples were recorded to determine the resolution, which is ultimately limited by the finite drift-suppression capability of r_i In the given lighting situation (590 nm LED), a maximum Signal to Noise Ratio of 15.5 Bits (at 1 Hz) and a maximum measurement rate of 1.9 kHz can be achieved Even higher measurement rates can be reached at higher light intensities. In Table I, this work is compared with other studies, with a focus on explicitly high precision. Two main types of angle sensors can be distinguished: digital sensors, which rely on pixel-based spatial resolution and center-of-gravity calculations between pixels, and analog sensors, which evaluate angle-dependent photocurrents, such as those induced by the shadow projection distance on a photodiode. In contrast to others, the proposed sensor system achieves the highest precision, with a $0.84m^\circ$ error at 3-sigma. Additonal this sensor principle is fully monolithically integrated and does not require post-processing in the optics [7]

TABLE I: Performance Comparison of optical angle Sensors

	this work	Koch[6]	Xie[7]	Ortega[1]
Sensor Type	differential Diodes	differential Diodes	APS	differential Diodes
non-integrated elements	-	-	optic	optic and circuitry
Technology [nm]	180	250	180	-
Power Supply [V]	3.3	–	$3.3/1.8$	-
Power consumption	$3mW$[a]	$1mW$	$42.73mW$	-
Photodiode Size[b] $[mm^2]$	0.538	0.285	0.394	2.4
FOV (Field of View)	13°	140°	94°	120°
Precision[c]	$0.84m^\circ$	$124m^\circ$	$10m^\circ$	$100m^\circ$
SNR[d] [Bit]	$15.5-9$	11.7	14.78	11.8
Measurement Rate [Hz]	$1-1.9k$	10	10	-
Wavelength [nm]	590	720	sunlight	sunlight

[a] without FPGA; [b] related to one axis; [c] 3-Sigma; [d] FOV/Precision (1-Sigma)

or external discrete evaluation circuitry [1]. Given the higher calculation frequency of r_i compared to [7] (which corresponds to a higher measurment rate), the circuit demonstrated here exhibits superior suppression of 1/f noise and drift effects. Thus enables long-term averaging over a large number of individual measurements over e.g. a period of up to one second, resulting in exceptional overall accuracy. Additionally, the sensor system eliminates the influence of brightness (and any PVT) variations by calculating the relativ related difference r_i.

IV. Conclusion

This paper presents a monolithically integrated angle sensor with exceptional precision that is specially optimized for transmitted light refractometer applications. The sensor achieves a precision of $0.84m^\circ$. The sensing principle employed offers considerable flexibility, both in terms of measurement rate and resolution. In addition, the overall concept is absolutely robust against any kind of PVT fluctuations. In conjunction with the techniques already presented in earlier publications, it also enables the use of point light sources at a great distance as well as those at close range with a strong gradient within the light cone [4], [5].

References

[1] P. Ortega, G. López-Rodríguez, J. Ricart, M. Domínguez, L. M. Castañer, J. M. Quero, C. L. Tarrida, J. García, M. Reina, A. Gras, and M. Angulo, "A miniaturized two axis sun sensor for attitude control of nano-satellites," *IEEE Sensors Journal*, vol. 10, no. 10, pp. 1623–1632, 2010.

[2] L. Farian, P. Häfliger, and J. A. Leñero-Bardallo, "A miniaturized two-axis ultra low latency and low-power sun sensor for attitude determination of micro space probes," *IEEE Transactions on Circuits and Systems I: Regular Papers*, vol. 65, no. 5, pp. 1543–1554, 2018.

[3] C. Constantin and S. Bucharest, "Process electronic refractar meter in a compact structure," in *2006 IEEE International Conference on Automation, Quality and Testing, Robotics*, vol. 2, 2006, pp. 133–136.

[4] A. Feiler, D. Veit, L. Straczek, and J. Oehm, "Conceptual study for ultra miniaturized high-precision optical cmos sensors unaffected by gradients in illumination," in *2019 15th Conference on Ph.D Research in Microelectronics and Electronics (PRIME)*, 2019, pp. 153–156.

[5] J. Oehm, C. Koch, I. Stoychev, and A. Gornik, "Improved high precision optical angle measurement system with no interference of light gradients and mismatch," in *2012 19th IEEE International Conference on Electronics, Circuits, and Systems (ICECS 2012)*, 2012, pp. 209–212.

[6] C. Koch, J. Oehm, and A. Gornik, "High precision optical angle measuring method applicable in standard cmos technology," in *2009 Proceedings of ESSCIRC*, 2009, pp. 244–247.

[7] N. Xie and A. J. P. Theuwissen, "A miniaturized micro-digital sun sensor by means of low-power low-noise cmos imager," *IEEE Sensors Journal*, vol. 14, no. 1, pp. 96–103, 2014.